Magnetic-field-induced transitions and evolution of magnetotransport properties in quasi-two-dimensional KMo_6O_{17} in the charge-density-wave phase

J.-F. Wang,[1,*] M. Yang,[1] L. Li,[1] M. Sasaki,[2] A. Ohnishi,[2] M. Kitaura,[2] K.-S. Kim,[3] and Heon-Jung Kim[4,†]

[1]*Wuhan National High Magnetic Field Center (WHMFC), Huazhong University of Science and Technology, Wuhan 430074, China*

[2]*Department of Physics, Faculty of Science, Yamagata University, Kojirakawa, Yamagata 990-8560, Japan*

[3]*Department of Physics, Pohang University of Science and Technology (POSTECH), Pohang, Gyeongbuk 790-784, Republic of Korea*

[4]*Department of Physics, College of Natural Science, Daegu University, Gyeongbuk 712-714, Republic of Korea*

(Received 4 October 2013; revised manuscript received 17 December 2013; published 23 January 2014)

Longitudinal magnetoresistivity $\rho_{xx}(B)$ and Hall resistivity $\rho_{xy}(B)$ of KMo_6O_{17} single crystals have been measured up to 60 T in a pulse magnet. Remarkable and unusual features at characteristic magnetic fields were found in both $\rho_{xx}(B)$ and $\rho_{xy}(B)$, which were attributed to Fermi surface reconstructions caused by field-induced density-wave transitions. To understand these transitions in detail, we analyzed $\rho_{xx}(B)$ and $\rho_{xy}(B)$ based on a multiband model. This model successfully described the experimental results, revealing that charge carriers are increased significantly at these transitions with increasing magnetic field as a result of the Fermi surface reconstruction. In particular, the charge carriers are increased by two orders of magnitude at $B_{osc} = \sim 40$ T, above which a quantum oscillation emerges in both $\rho_{xx}(B)$ and $\rho_{xy}(B)$. This strongly suggests that the field-induced quantum oscillation is closely related with the induced charge carriers.

DOI: 10.1103/PhysRevB.89.035137 PACS number(s): 72.15.Gd, 72.20.Ht, 73.20.Mf

I. INTRODUCTION

The fate of a metal or a doped semiconductor in a strong magnetic field is an interesting but yet unresolved problem in physics. In two-dimensional (2D) electron gas, the formation of Landau levels leads to the integer [1] or fraction quantum Hall effect [2,3]. In a three-dimensional (3D) metal with a spherical Fermi surface, Landau quantization modifies the wave functions into Landau levels in a plane perpendicular to the magnetic field while the plane-wave-like character is maintained in the parallel direction. As the magnetic field increases, the so-called quantum limit is reached, where all electrons occupy the lowest Landau level. Beyond this quantum limit, instability toward novel electronic order is expected to appear.

In a real system, not only the Landau quantization but also the band structure plays an important role in determining the ground state at a strong magnetic field. For instance, in graphite, a typical layered semimetal with very high anisotropy, eight relevant Landau subbands were predicted to govern the low-energy physics at a strong magnetic field [4]. Above the quantum limit, where only the lowest electron and hole subbands are populated, a density-wave (DW) state is known to be stabilized [5–7]. This is a consequence of the quasi-one-dimensionality of the energy spectrum caused by Landau quantization and strong correlation [6,7]. Interestingly, this DW state is destabilized at even higher magnetic fields due to crossing of a Landau subband at the Fermi level [7]. Later study reveals that magnetic field, in fact induces two successive phase transitions, dividing two distinct DW states before a metallic phase is finally stabilized [8].

Change of the DW instability in a magnetic field can be more clearly visible in a quasi-one-dimensional (Q1D) system. Theoretical studies have considered the influence of the external magnetic field on the change of the charge DW (CDW) properties such as the critical temperature and the nesting wave vector [8–10]. An external magnetic field couples to the spin and orbits of the electrons via Zeeman term and Peierls substitution in Hamiltonian, respectively. When the orbital effect is dominant, new DW instability emerges at the wave vectors different from the original one, at which the spin susceptibility becomes maximum and the zero-field Fermi area is quantized in terms of $A_0 = 2\pi eB$, where B is the magnetic field [8]. On the other hand, the effect of the Zeeman term is more complex. It mixes the CDW and the induced spin DW (SDW) by the magnetic field, shifting the wave vector of instability. Depending on the relative strength of the Zeeman and orbital terms, a rather complex phase diagram with different DW order has been predicted [10]. In fact, this theoretical picture has been a qualitative basis to interpret the field-induced transitions observed in low-dimensional systems at high magnetic fields [11–13].

KMo_6O_{17}, which is called the purple bronze, is a typical system that possesses the features mentioned above. It is a quasi-2D metal with a trigonal structure including MoO_6 octahedra layers separated by K^+ ions and MoO_4 tetrahedra [14–22]. Its Fermi surfaces (FSs) consist of two electron pockets at Γ and one hole pocket at L for the partially filled d bands with no apparent nesting character in the first Brillouin zone [14,15]. The nesting property is in fact "hidden" and it is only visible when three FSs are viewed as a combination of three pairs of Q1D Fermi sheets [14]. Indeed, the CDW instability is revealed as a sudden upturn at $T_{c1} \sim 110$ K in the temperature dependence of the zero-field resistivity [16]. Another upturn possibly caused by another CDW or new SDW instability is also seen at $T_{c2} \sim 25$ K. It is expected that most FSs are gapped out, and small residual electron and hole FSs remain in the CDW state.

At low temperatures below T_{c2}, the in-plane and interlayer magnetoresistance (MR) as well as the magnetic torque in a magnetic field up to 30 T, perpendicular to the conducting layers have detected several characteristic magnetic fields,

*jfwang@mail.hust.edu.cn

†Corresponding author: hjkim76@daegu.ac.kr

which were presumably assigned to be successive field-induced DW transitions [17]. More interestingly, a quantum oscillation in the interlayer MR begins to appear at around 40 T [17], reminiscent of the so-called kink transition in the Q2D organic conductors [23,24] or of the field-induced quantum oscillation in the Q2D blue bronze η-Mo_4O_{11} [25,26]. This may indicate field-induced closing of a charge gap and it seems to be a universal feature of purple bronze compounds because $Li_{0.9}Mo_6O_{17}$ is also known to exhibit a similar behavior [27]. Despite this phenomenology, the microscopic mechanism for the field-induced transitions has not been understood yet in detail. In particular, how FS is reconstructed across the field-induced transitions is unknown due to lack of such information as mobility and carrier density with magnetic fields, which could be obtained via MR and Hall resistance measurements. The simultaneous measurements of these quantities at high magnetic fields have been hampered owing to small signals and technical complexity of their measurements in the pulse-field measurement. In this paper, we report simultaneous measurements and analysis of the MR and Hall resistance up to 60 T with a pulse magnet. These data are analyzed based on a multiband model. Our analysis clearly shows how these quantities evolve across these characteristic fields, providing an important clue about FS reconstructions.

II. EXPERIMENT

The single crystals used in this study were grown by electrolytic reduction of a melt of K_2CO_3-MoO_3 with a suitable molar ratio [28]. The crystals were characterized by the single-crystal x-ray diffraction and electrical resistivity measurements, and were found to possess good quality. The plateletlike samples were cut into bar shapes of appropriate geometry for MR and Hall resistance measurements. The MR and Hall resistance from these single crystals exhibited consistent results with the data in the literatures. The measurements of the MR and Hall resistance were carried out simultaneously in pulsed magnetic fields up to 60 T with the pulse duration of 50 msec in Wuhan National High Magnetic Field Center. For this purpose, five contacts with Hall bar shape were carefully made by using a silver paste. The contact resistances were maintained to be small, which is essential for good signal-to-noise ratio in a pulsed magnetic field. The stability of the pulse magnetic fields and the low contact resistances enabled us to obtain even the small Hall resistance very reproducibly. We applied ac current with small amplitude and detected the response MR and Hall voltages by using a high-performance DAQ instrument. We also compared the results obtained by this ac technique with the ones from a conventional dc method and found that both methods produce the same results with superior data quality in the ac technique.

III. RESULTS AND DISCUSSION

Figure 1 presents the schematic pictures of FSs in the normal state ($T > T_{c1}$) as well as the expected electron and hole pockets in the CDW state. In the normal state, there are two electron and one hole pockets centered at Γ and L, respectively. The dashed (green) lines emphasize a pair of the hidden Q1D nesting feature. It is expected that at low

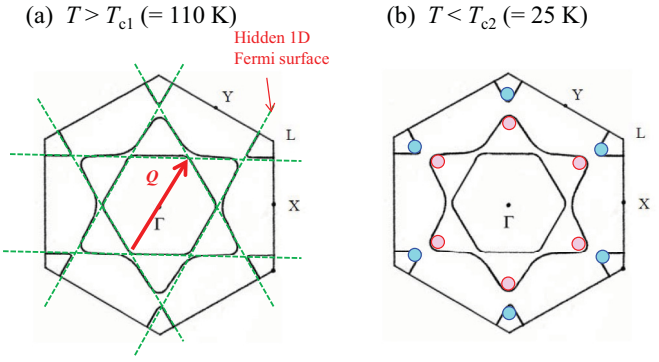

FIG. 1. (Color online) (a) A schematic picture for Fermi surfaces and the hidden one-dimensional nesting feature of KMo_6O_{17} at high temperatures for $T > T_{c1}$. The (red) arrow indicates the nesting wave vector. (b) The electron and hole pockets expected to remain in the second CDW/SDW phase at $T < T_{c2}$.

temperatures, the nested parts in this pair are gapped out and only small area remains in the CDW state as depicted in Fig. 1(b). This expectation is consistent with metallic zero-field resistivity below T_{c1}. At present, the shape and distribution of FSs in the k space is unknown at low temperatures but the FS reconstruction occurs two times successively with decreasing temperature; one at T_{c1} and the other is at T_{c2}. The second anomaly at T_{c2} in resistivity was suggested to be another DW instability. Nonetheless, it is likely that such a pair of electron and hole pockets depicted in Fig. 1(b) exists below T_{c2} although the size of the pockets and the number of the pairs are not known precisely.

Figures 2(a) and 2(b) show longitudinal resistivity ρ_{xx} and Hall resistivity ρ_{xy}, respectively, at fixed temperatures below T_{c2} as a function of the magnetic field B up to 60 T. Both ρ_{xx} and ρ_{xy} increase with B with very large MR $\{= [\rho_{xx}(B) - \rho_{xx}(0)]/\rho_{xx}(0)\}$ up to $B = \sim 20$ T and then they decrease above this field. The large MR implies that the residual electron and hole bands are nearly compensated. Another notable feature in these data is the existence of anomalies at four characteristic magnetic fields, which are indicated by the (blue and red) arrows. In fact, these anomalies observed in $\rho_{xx}(B)$ and $\rho_{xy}(B)$ in the present study are similar to the ones identified in the interlayer resistivity measurements [17]. The four characteristic magnetic fields from low B in

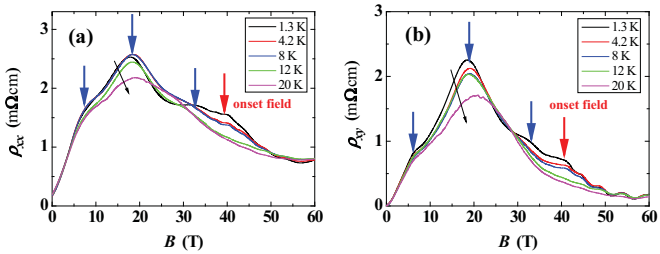

FIG. 2. (Color online) Magnetic field dependencies of (a) ρ_{xx} and (b) ρ_{xy} measured at several fixed temperatures for $T < T_{c2}$. The (black) arrows indicate temperature increase. We identify the characteristic magnetic fields of $B_2 \sim 7$ T, $B_3 \sim 20$ T, $B_{on} \sim 30$ T, $B_{osc} \sim 40$ T in ρ_{xx} (B) and (b) $\rho_{xy}(B)$ curves.

the present study correspond well to B_2, B_3, B_{on}, and B_{osc}, identified in Ref. [17] and thus, we also use the same notations. One important difference is that although there was no clear anomaly at B_{osc} in the previous interlayer resistivity, a kink is seen clearly in ρ_{xx} and ρ_{xy}. It is noted that four anomalies appear at the same magnetic fields in both ρ_{xx} and ρ_{xy}, which suggests that these features present changes of electronic structures at the corresponding magnetic fields. In the previous studies, B_2, B_3, and B_{on} were attributed to the field-induced DW transitions [17]. This interpretation is consistent with theoretical predictions in a Q1D system about the shifts of the density wave vector at high B. This effect depends on the ratio of the orbital to the Zeeman coupling and on the transverse interchain coupling. In the previous study, the phase above B_{on} was speculated to be a DW state with reduced gaps, which could be originated from the strong Zeeman contribution.

The evolution of the characteristic magnetic fields with increasing temperature can be seen also in Figs. 2(a) and 2(b). While the features at B_2 and B_3 are quite robust against the temperature change up to 20 K, the ones at B_{on} and B_{osc} become quickly broadened with increasing temperature. In the previous study, the features at B_3 and B_{on} were reported to be merged [17]. As the feature at B_{on} is quite broadened at higher temperatures, it is not so clear whether the features at B_3 and B_{on} are merged or the feature at B_3 is disconnected above T_{c2}. The peaklike feature at B_3 exhibits strongest temperature dependence compared with other features.

It is quite interesting that both ρ_{xx} and ρ_{xy} decrease above B_3. In a simple one-band picture, the change of the sign in the slop of $\rho_{xy}(B)$ implies the change of the carrier type. However, as KMo_6O_{17} is a multiband system in the CDW state, possessing both electron and hole FSs, this simple picture cannot be applied and one should consider a multi-band model for ρ_{xx} and ρ_{xy}. In the multiband model, ρ_{xx} and ρ_{xy} are determined by the mobility and carrier density of all the charge carriers. Therefore the $\rho_{xx}(B)$ and $\rho_{xy}(B)$, in principle, contain information about the evolution of the mobility and the carrier density with B as well as with temperature.

More quantitatively, $\rho_{xx}(B)$ and $\rho_{xy}(B)$ in the multiband model [29,30] are given by

$$\rho_{xx} = \frac{A}{A^2 + N^2 B^2} \quad \text{and} \quad \rho_{xy} = \frac{NB}{A^2 + N^2 B^2}, \tag{1}$$

and

$$A = \sum_i \frac{n_i e \mu_{ei}}{1 + \mu_{ei}^2 B^2} + \sum_j \frac{p_j e \mu_{hj}}{1 + \mu_{hj}^2 B^2} \quad \text{and}$$
$$N = \sum_i \frac{n_i e \mu_{ei}^2}{1 + \mu_{ei}^2 B^2} + \sum_j \frac{p_j e \mu_{hj}^2}{1 + \mu_{hj}^2 B^2}, \tag{2}$$

where n_i and p_j are the ith electron and jth hole concentrations, respectively, e is the elementary charge, and μ_{ei} and μ_{hj} are the corresponding mobility. In fact, this model was successfully utilized to explain the B dependence of the MR and Hall voltage in η-Mo_4O_{11} [29]. Thus this model can allow us to extract the values of the mobility and the carrier density in different field-induced phases at high magnetic fields.

To compare the experimental results with the formula more quantitatively, the followings are assumed about the high-field phases. First, the number of the electron FSs is approximately same as that of the hole FSs and the high-field phases are nearly compensated ($n_i \approx p_i$) as in the zero-field phase. Second, as a result of a field-induced transition, additional electrons and holes emerge above each corresponding magnetic field. As these transitions are not sharp even at $T = 1.3$ K, the increase of the electron and hole carriers is parameterized phenomenalistically by a broadened step function of $n_i(B) = n_{i0}/\{1 + \exp[-(B - B_i)/\alpha_i]\}$, where n_i and B_i are the carrier density and the characteristic field, respectively, and α_i corresponds to the transition width. Third, since a distinct feature can be identified in B_{osc}, above which quantum oscillations are observed in both $\rho_{xx}(B)$ and $\rho_{xy}(B)$, we also assume that FS is modified at B_{osc},.

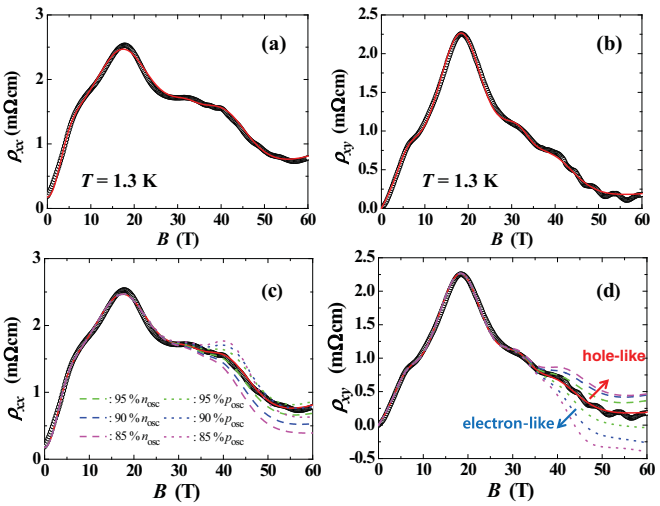

FIG. 3. (Color online) Simulated curves for (a) ρ_{xx} and (b) ρ_{xy} based on a multiband model along with experimental results at $T = 1.3$ K. Please see the main text for details. Simulated curves for (c) ρ_{xx} and (b) ρ_{xy} at $T = 1.3$ K with 95%, 90%, and 80% of the optimal hole (electron) density above B_{osc}. These curves show that the condition for the carrier compensation is still satisfied above B_{osc}.

Figures 3(a) and 3(b) are the simulated $\rho_{xx}(B)$ and $\rho_{xy}(B)$, together with the experimental data, respectively. The simulated results reproduce the experimental data quite well. Particularly, the regions near the characteristic magnetic fields are well described. In this simulation, we used the mobility values of $\mu_e = 0.1 - 0.5$ m^2/Vs and $\mu_h = 0.5 - 1.0$ m^2/Vs. In fact, as our model contains several parameters such as the mobility, the carrier density, and the width α_i, the simulation with different set of parameters might give rise to a similar shape of simulated curves. However, we found that when important parameters such as the carrier density and mobility are modified significantly, the shapes of the resultant curves are changed completely. Although a small change in the carrier density and mobility could lead to small change in the $\rho_{xx}(B)$ and $\rho_{xy}(B)$ curves, the overall trend such as total carrier density with B is preserved. Importantly, it is observed that the induced carrier density increases significantly at B_2, B_3, B_{on}, and B_{osc}. These increases are not modeled by a change of mobility when the carrier density is kept to be small within a physically reasonable range of the mobility values. Particularly, as the carrier density increases enormously at

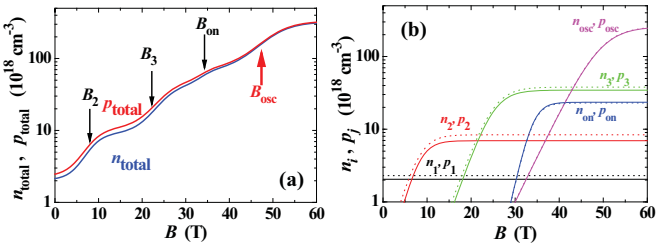

FIG. 4. (Color online) Magnetic field dependencies of (a) total electron and hole concentrations and (b) their component concentration. The solid and dashed lines represent the electron and hole concentrations, respectively. The n_1 (p_1) is the electron (hole) concentration below B_2. The n_2 (p_2), n_3 (p_3), n_{on} (p_{on}), and n_{osc} (p_{osc}) are the electron (hole) concentrations induced at B_2, B_3, B_{on}, and B_{osc}, respectively.

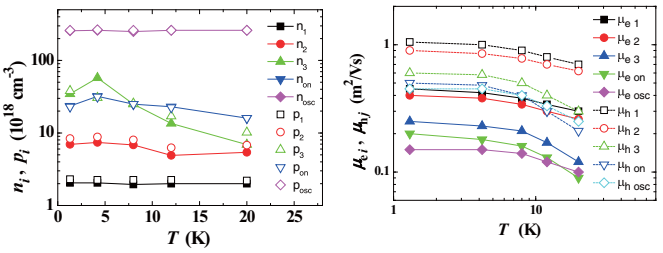

FIG. 5. (Color online) (a) Temperature dependencies of the electron (hole) concentrations of n_1 (p_1). The n_2 (p_2), n_3 (p_3), n_{on} (p_{on}), and n_{osc} (p_{osc}) and (b) temperature dependencies of their mobility values.

B_{osc}, the carrier compensation needs to be checked at the high field region. Figures 3(c) and 3(d) present the simulation results obtained as the hole or electron carrier density is decreased successively by 5%. The simulation curve above B_{osc} is very sensitive to unbalance of the hole and electron charge carriers, which confirms that the charge carriers are indeed compensated above B_{osc}.

The total and induced carrier densities with increasing B are summarized in Figs. 4(a) and 4(b), respectively. The total electron carrier density is $\sim 2 \times 10^{18}$ cm^{-3} at $B = 0$ T. It increases drastically at B_2, B_3, and B_{osc}, reaching $\sim 3 \times 10^{20}$ cm^{-3} at $B = 60$ T. It is notable that a huge number of the carriers are induced at B_{osc}, above which quantum oscillations are clearly visible in both $\rho_{xx}(B)$ and $\rho_{xy}(B)$ curves. This observation suggests a possible origin of these quantum oscillations. Interestingly, the $\rho_{xy}(B)$ exhibits a clearer oscillation than the $\rho_{xx}(B)$ and that oscillation is as pronounced as the ones observed in the interlayer resistivity with similar oscillation period in $1/B$. As the appearance of the quantum oscillation is clearly related to the field-induced increase of the charge carrier, its absence could be due to the deficiency of the charge carriers below B_{osc}. According to the Onsager relation, $\Delta(1/B) = 2\pi e/(\hbar c S)$, where S is the area of the FS normal to the direction of B, the distance between two successive maximum in B becomes larger as the carrier density decreases. This distance might be larger than the distance in B between two field-induced transitions.

It seems that there is correlation between the increase of the carrier density and the appearance of quantum oscillation above B_{osc}. The oscillation frequency $\Delta(1/B)$ is measured to be 468 T, which corresponds to the extremal area of the FS of 4.46 nm^{-2}. This is about 5% of total areas including all three FSs shown in Fig. 1. On the other hand, the carrier density deduced from the multiband analysis above B_{osc} can be compared with the one expected from the original FSs at high temperatures. By using the fractional areas of three FSs with respect to the Brillouin zone, we find that the electron carrier density of 3×10^{20} cm^{-3} obtained in the mutiband analysis is only about 10% of the expected value from the FSs, which suggests that all the carriers at high temperatures and at low fields are not recovered even above B_{osc}. Considering that the multiband analysis only estimates the order of magnitude of the carrier density, its result is consistent with the frequency of the quantum oscillation observed above B_{osc}.

Although the origin of the field-induced oscillation is not clear at present, we would like to emphasize that similar phenomena have been observed in the Q2D organic conductor (BEDT-TTF)$_2$KHg(SCN)$_2$ and in η-Mo$_4$O$_{11}$ which is a sister compound of KMo$_6$O$_{17}$ in terms of crystalline and electronic structures. In (BEDT-TTF)$_2$KHg(SCN)$_2$, the field-induced oscillation is closely related with the so-called kink transition, which appears as a sudden decrease in MR [23,24]. This transition was suggested to emerge due to vanishing of an overlap between neighboring Landau subbands. Because of well-defined Landau subbands, the oscillations might appear above the kink transition and this may explain concomitant appearance of the quantum oscillation. On the other hand, the similar phenomenon in η-Mo$_4$O$_{11}$ was explained based on charge transfer with magnetic breakdown between the electron band and hole Landau levels [26]. As KMo$_6$O$_{17}$ resembles η-Mo$_4$O$_{11}$ in several aspects, it is reasonable to speculate that the same mechanism may explain the oscillations in KMo$_6$O$_{17}$. However, one should be also cautious because a quantum oscillation depends on very details of FS structure. Therefore more detailed investigation on this problem will be necessary in near future to understand the origin of the field-induced oscillation in KMo$_6$O$_{17}$.

We apply same analysis to the experimental results at higher temperatures and obtained the temperature dependence of the carrier density and mobility. Figure 5(a) presents the temperature dependence of the electron and hole carrier densities up to $T = 20$ K, showing that all the carrier densities except for the induced one at B_3 are nearly temperature-independent. This temperature independence is understandable because usually the electronic structure does not change with temperature. On the other hand, the carrier densities related with B_3 decrease with temperature in the range of 1.3 K $\leq T \leq$ 20 K, which renders us to speculate that this field-induced transition is closely linked with the second CDW/SDW transition at $T_{c2} = 25$ K. Strong temperature dependence of the features at B_3 even in the raw data seems to reflect this connection without the quantitative analysis. As shown in Fig. 5(b), the mobility values are found to decrease slightly with increasing temperature, which is reasonable considering inelastic scatterings of the electrons and holes with elementary excitations such as phonons.

As the features of $\rho_{xx}(B)$ and $\rho_{xy}(B)$ at the characteristic magnetic fields are delineated as phase boundaries between

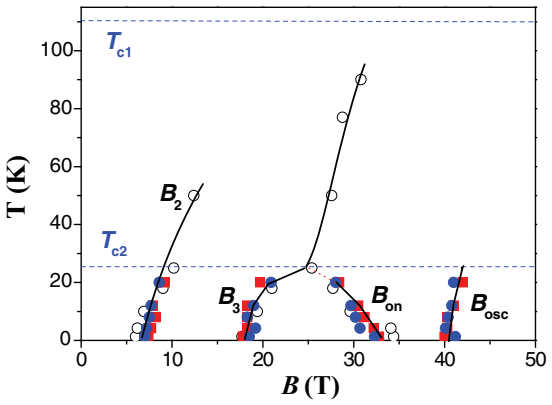

FIG. 6. (Color online) The B-T phase diagram showing characteristic field, B_2, B_3, B_{on}, and B_{osc} at different temperatures. The open circles are the characteristic fields extracted from $\rho_{xx}(B)$, which is measured by the dc method. The closed (red) rectangles and (blue) circles are B_2, B_3, B_{on}, and B_{osc} from $\rho_{xx}(B)$ and $\rho_{xy}(B)$, respectively, which are measured by the ac technique.

different CDW/SDW, accompanying the change of the charge carriers, it is natural to summarize those characteristic magnetic fields in the B-T plane in Fig. 6. We include not only the characteristic fields from the $\rho_{xx}(B)$ and $\rho_{xy}(B)$ curves measured by the ac technique, but also the ones from the $\rho_{xx}(B)$ curves measured by the dc method, which will be reported elsewhere in Fig. 6. While both B_2 and B_3 survive above T_{c2}, B_{osc} does not. In addition, it is not so clear whether B_{on} is merged with B_3 or it is disconnected above T_{c2}. In any case, the B-T phase diagram in Fig. 6 shows that B_3, B_{on}, and B_{osc} are intimately connected with the second CDW/SDW transition at T_{c2}.

Finally, we remark on the previous study on AMo_6O_{17} (A = Na, K, and Tl) [19], where MR's for the magnetic fields of B//c and $B\perp$c were analyzed based on a two-band model. Although their approach is similar to ours, our estimated values of the parameters are believed to be more reliable because the MR and Hall resistance, which are sensitive to mobility and carrier density, respectively are compared with the model. In addition, we cover much wider ranges of the magnetic fields.

IV. CONCLUSION

In conclusion, we have conducted simultaneous measurements of longitudinal magnetoresistance and Hall resistance for KMo_6O_{17} in the charge-density-wave phase up to $B = 60$ T in a pulse magnet. Four anomalies at characteristic magnetic fields were observed in these measurements, whose origin could be attributed to Fermi surface reconstructions caused by field-induced density-wave transitions. To extract the evolution of carrier density and mobility with magnetic field, these experimental data were analyzed based on a multi-band model. This also shows that magnetoresistance and Hall resistance with magnetic field can be understood quantitatively by the influence of electrons and holes induced at characteristic magnetic fields.

ACKNOWLEDGMENTS

H.-J.K was supported by Basic Science Research Program and National Nuclear R&D Program through the National Research Foundation of Korea (NRF) funded by the Ministry of Education, Science, and Technology (No. NRF-2010-0021438 and NRF-2012M2B2A4029488). Part of this work was supported by the National Natural Science Foundation of China (Grant No. 10904044).

[1] K. v. Klitzing, G. Dorda, and M. Pepper, Phys. Rev. Lett. **45**, 494 (1980).
[2] D. C. Tsui, H. L. Stormer, and A. C. Gossard, Phys. Rev. Lett. **48**, 1559 (1982).
[3] R. B. Laughlin, Phys. Rev. Lett. **50**, 1395 (1983).
[4] K. Nakao, J. Phys. Soc. Jpn. **40**, 761 (1976).
[5] D. Yoshioka and H. Fukuyama, J. Phys. Soc. Jpn. **50**, 725 (1981).
[6] Y. Takada and H. Goto, J. Phys.: Condens. Matter. **10** 11315 (1998).
[7] H. Yaguchi and J. Singleton, Phys. Rev. Lett. **81**, 5193 (1998).
[8] Benoît Fauqué, David LeBoeuf, Baptiste Vignolle, Marc Nardone, Cyril Proust, and Kamran Behnia, Phys. Rev. Lett. **110**, 266601 (2013).
[9] G. Montambaux, M. Héritier, and P. Lederer, Phys. Rev. Lett. **55**, 2078 (1985).
[10] D. Zanchi, A. Bjeliš, and G. Montambaux, Phys. Rev. B **53**, 1240 (1996).
[11] S. Uji, M. Kimata, S. Moriyama, J. Yamada, D. Graf, and J. S. Brooks, Phys. Rev. Lett. **105**, 267201 (2010).
[12] A. G. Lebed and Si Wu, Phys. Rev. Lett. **99**, 026402 (2007).
[13] D. Graf, E. S. Choi, J. S. Brooks, M. Matos, R. T. Henriques, and M. Almeida, Phys. Rev. Lett. **93**, 076406 (2004).
[14] M.-H. Whangbo, E. Canadell, P. Foury, and J.-P. Pouget, Science **252**, 96 (1991).
[15] G.-H. Gweon, J. W. Allen, J. A. Clack, Y. X. Zhang, D. M. Poirier, P. J. Benning, C. G. Olson, J. Marcus, and C. Schlenker, Phys. Rev. B **55**, R13353 (1997).
[16] A. Rotger, C. Schlenker, J. Dumas, J. Marcus, S. Dubois, A. Audouard, L. Brossard, J.P. Ulmet, and S. Askenazy, Synth. Met. **56**, 2725 (1993).
[17] J. Dumas, H. Guyot, H. Balaska, J. Marcus, D. Vignolles, I. Sheikin, A. Audouard, L. Brossard, and C. Schlenker, Physica B **346-347**, 314 (2004).
[18] H. Guyot, J. Dumas, M. V. Kartsovnik, J. Marcus, C. Schlenker, I. Sheikin, and D. Vignolles, Eur. Phys. J. B **58**, 25 (2007).
[19] M. Tian, S. Yue and Y. Zhang, Phys. Rev. B **65**, 104421 (2002).
[20] X. Qin, J. Shi, H. Gong, M. Tian, J. Wei, H. Chen, and D. Tian, Phys. Rev. B **53**, 15538 (1996).
[21] Xiaofeng Xu, A. F. Bangura, C. Q. Niu, M. Greenblatt, Song Yue, C. Panagopoulos, and N. E. Hussey, Phys. Rev. B **85**, 195101 (2012).
[22] Ming-Liang Tian, Song Yue, Shiyan Li, Yuheng Zhang, and Jing Shi, J. Appl. Phys. **89**, 3408 (2001).

[23] T. Osada, R. Yagi, A. Kawasumi, S. Kagoshima, N. Miura, M. Oshima, and G. Saito, Phys. Rev. B **41**, 5428 (1990).
[24] C. Proust, A. Audouard, A. Kovalev, D. Vignolles, M. Kartsovnik, L. Brossard, and N. Kushch, Phys. Rev. B **62**, 2388 (2000).
[25] S. Hill, S. Valfells, S. Uji, J. S. Brooks, G. J. Athas P. S. Sandhu, J. Sarrao, Z. Fisk, J. Goettee, H. Aoki, and T. Terashima, Phys. Rev. B **55**, 2018 (1997).
[26] K. Suga A. Ohnishi, M. Koyano, M. Sasaki, and K. kindo, J. Phys. Soc. Jpn. **77**, 074605 (2008).
[27] Xiaofeng Xu, A. F. Bangura, J. G. Analytis, J. D. Fletcher, M. M. J. French, N. Shannon, J. He, S. Zhang, D. Mandrus, R. Jin, and N. E. Hussey, Phys. Rev. Lett. **102**, 206602 (2009).
[28] J. F. Wang, R. Xiong, D. Yin, C. Z. Li, Z. Tang, Q. Q. Wang, J. Shi, Y. Wang, and H. H. Wen, Phys. Rev. B **73**, 193102 (2006).
[29] M. Inoue, G. Marcel, I. Laue, M. von Ortenberg, and M. Sasaki, Phys. Status Solidi B **172**, 431 (1992).
[30] M. Sasaki, Y. Hara, M. Inoue, T. Takamasu, N. Miura, G. Machel, and M. von Ortenberg, Phys. Rev. B **55**, 4983 (1997).